

Coordination Strategy for Digital Frequency Relays and Energy Storage in a Low-Inertia Microgrid

Sayed M. Said^{a,*}, Emad A. Mohamed^a, Bálint Hartmann^b

^aDepartment of Electrical Engineering, Faculty of Engineering, Aswan University, Aswan 81542, Egypt

^bDepartment of Electric Power Engineering, Budapest University of Technology and Economics, 1111 Budapest, Hungary

Abstract

Recently, dynamic frequency stability problems have started to arise in microgrid systems with the increasing utilization of low inertia and intermittent renewable energy sources. This leads to limiting the maximum penetration of renewable sources in microgrids. In order to solve this problem and increase the penetration of renewable sources, the dynamic frequency controller of the microgrid should be enhanced. Therefore, this paper will provide virtual inertia response of superconducting magnetic energy storage coordinated with the load frequency control depending on a new optimal proportional-integral-derivative controller-based advanced swarm intelligence technique, named Moth Swarm Algorithm (MSA). Moreover, the proposed inertia control strategy is coordinated with digital frequency relay to enhance dynamic frequency stability and maintain microgrid dynamic security at high penetration levels of renewable sources and radical load change. To attest the superiority of the proposed technique, it has been examined using MATLAB/SIMULINK, considering different contingency cases and varying the inertia level of the studied microgrid. The results stated that the proposed coordination can effectively regulate microgrid frequency and maintain dynamic stability and security.

Keywords: digital protection; load frequency control; low-inertia microgrid; superconducting magnetic energy storage

Introduction

Reliable operation of microgrids (MGs) in modern power systems have become a major concern due to the progressive employment of renewable energy sources (RES) (i.e., wind turbines and photovoltaic (PV) arrays) as power generation units instead of conventional synchronous generators [1]. The high penetration of these RES units has brought many challenging issues regarding protection and stability aspects of MGs, particularly frequency stability due to the lack of inertia, which leads to frequency excursions (i.e., large fluctuations of loads or tripping of generation units) [2]. Consequently, MGs suffer from a lack of frequency/voltage stabilization relative to conventional synchronous generators [3]. Hence, the MG system could become unsafe as RES penetration levels increase, in addition to imbalances occurring between generation and demand where dynamic frequency stability is problematic.

In order to solve these problems related to low-inertia MGs, several papers discuss control techniques such as virtual inertia control (VIC) [4]. VIC is used to imitate the in-

ertia characteristics of prime movers and synchronous machines [5, 6]. In [7], the authors presented a comparative study of the dynamic characteristics between a virtual synchronous generator (VSG) and droop control techniques to mimic power system inertia. Reference [8] applied the VIC-based model predictive control method (MPC), where the stability performance of the (MG) is investigated with high penetration of RES. An estimation method of frequency response using VIC to enhance power system stability during high wind power integration is presented in [9]. Moreover, in [10, 11], the VIC-based fuzzy logic control system is applied to damp frequency deviations in the power system. Furthermore, Torres in [12] presented an approach of the self-tuning VSG for inertia and damping coefficients online by solving an optimization problem. It is not easy to achieve a successful trade-off between nominal and robust performance using the aforementioned control methods. Moreover, they do not take into consideration the uncertainty formulations in the control design [12, 13]. Therefore, it is difficult to assure robust performance and robust stability simultaneously for a wide range of disturbance events and uncertainties based on conventional control techniques [14].

On the other hand, several ideas provided the inertia response from the energy storage systems (ESS), which is

*Corresponding author

Email address: sayed.said@aswu.edu.eg (Sayed M. Said)

termed as virtual inertia. The main goal of using the ESS is to preserve the real power of the power system in a stable point by load leveling and alleviating the fluctuation of RES [15–17]. Abraham [18] added a battery with the PV system to reduce its variability. This is done by sending the PV power to a high pass filter and setting it as a reference power to the battery system. Thus, the battery provides a high part of the transient power and smoothes out the PV output power. Furthermore, Tamrakar [19] added the virtual inertia from the ESS. His control method is based on the difference in frequency value from nominal and rate of change of frequency (RoCoF). Others presented coordination of self-adaptive wavelet decomposition method and a two-level power to emulate the MG inertia in [20]. Moreover, in [21] the authors used the state of charge (SOC) as a feedback control signal for the ESS to activate pitch control. However, this control technique is not suitable for dealing with the sudden variation of wind power, which is a common contingency. Also, in [22] the authors considered the SOC by proposing an approach that divides the ESS control region. However, the compensation of wind power fluctuations is done only by ESS without any action from a wind turbine. This technique can adversely affect the lifetime of the ESS due to capacity-related problems.

The superconducting energy storage system (SMES) is one of the most important ESS techniques – and the preferred choice of ESS with RES applications – as it can exchange real and reactive power with the MG in a fast and flexible way and thus can enhance MG dynamic security [23]. Furthermore, it has the best efficiency, energy density and lifetime of all ESS [24]. Multiple and various research has explored SMES teamed up with RES. References [25, 26] used SMES to boost the performance in the power system of the doubly-fed induction generator (DFIG) based wind turbine. Regulating the voltage, real power, and reactive power exchange between the power system and squirrel-cage induction generator (SCIG) based wind turbine using SMES was presented in [27]. The authors in [28] discussed SMES as a new supplementary load frequency control (LFC) scheme.

From another aspect, various papers discussed these MG problems using control and protection coordination to maintain the dynamic security of MGs. Several studies handled this MG issue from the perspective of frequency protection problems such as [29, 30], which applied an intelligent computational technique for load leveling under faulted conditions. Furthermore, Reference [31] presented the RoCoF relay for MG protection during major frequency disturbances. Furthermore, in [32] a comparative study of vector surge relays and the RoCoF is presented for DGs protection. However, this technique faced a difficult situation, as the protective relays coordination design did not sense the islanding instants within the required timeframe. In [33], the proposed method of the RoCoF and the frequency relays for DGs protection is proposed. However, this presented technique did not damp the frequency oscillations within the acceptable limits of frequency due to the energizing of the OUFRR once the system frequency goes beyond the acceptable limits.

Table 1: MG parameters

Parameter	Value	Parameter	Value
D	0.015	KSMES	6
H	0.083	TSMES	0.03
T _g	0.1	GRC	20%
T _t	0.4	VU	0.3
TWT	1.5	VL	-0.3
TPV	1.8	R	2.4

This paper proposes the use of improved controller-based SMES, a new optimal PID controller and optimal LFC to improve the dynamic frequency stability of low-inertia MGs during various disturbances cases. To sum up, this paper aims to accomplish the following:

- To present a new optimization technique based on Moth Swarm Algorithm (MSA) to enhance the LFC of microgrid system during high penetration of RES.
- To propose new coordination of SMES, optimal LFC and DFR to improve the frequency stability of the islanded microgrid system.
- To study the response of SMES integration on DFR operation in the MG during the low inertia situation as well as variations of residential and industrial loads.
- To validate and verify the effectiveness of the proposed technique, compared with conventional methods.

Development of the Proposed MG Model

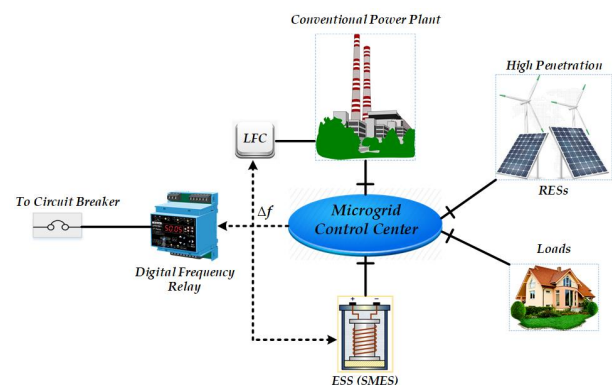


Figure 1: Simplified model of the studied MG

This study focuses on an islanded MG of 20 MW load base, which comprises 20 MW thermal power, 8 MW wind power, 4 MW solar power, 15 MW electrical loads and SMES

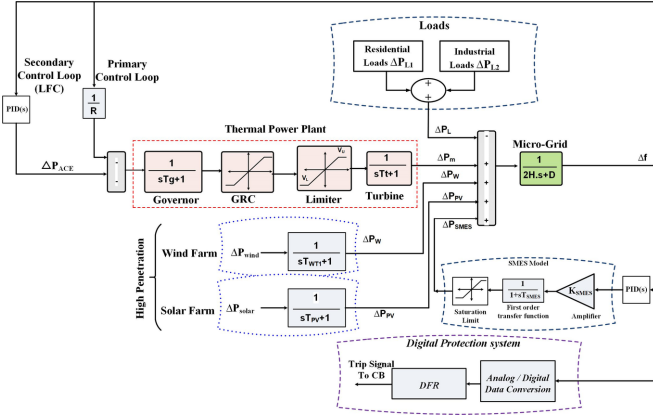


Figure 2: Frequency control model of the studied MG including RES and SMES

capacity of 5 MW. Fig. 1 shows a simplified model of the studied MG. This research takes into consideration the Generation Rate Constraints (GRC) of the thermal generation with limits as 0.2 pu MW/min for modeling the actual MG [14]. It also considers minimum and maximum limits (V_U , V_L) to restrict valve operations. Fig. 2 shows the dynamic model of the tested MG. All dynamic parameters of MG are summarized in Table 1.

State-Space model of the tested MG

MGs show time-varying and highly nonlinear characteristics. However, the impact of dynamic nature on the frequency response is slower than the effect on rotor and voltage dynamics. Hence, the low order linearized model is acceptable for the frequency control analysis. Eq. (1) gives a generalized model of the power balance equation for the MG in the case of load disturbance:

$$\Delta f = \frac{1}{2Hs + D} (\Delta P_m - \Delta P_L) \quad (1)$$

where frequency deviation (Δf) is due to the power mismatch ($\Delta P_m - \Delta P_L$), while D and H are the damping and inertia factors, respectively. In this equation, however, RES and SMES are not included. Fig. 2 shows the modified block diagram of the MG for frequency control purposes containing the primary, secondary, RES and SMES control loops. The modeling of the RES and SMES are explained in the following subsections and added to the linear model of the studied MG.

$$\Delta P_m = \frac{1}{sT_t + 1} (\Delta P_g) \quad (2)$$

$$\Delta P_g = \frac{1}{1 + sT_g} (\Delta P_{ACE} - \frac{1}{R} \Delta f) \quad (3)$$

$$\Delta P_{ACE} = \frac{ACE}{s} = \left[K_P + \frac{K_i}{s} + K_d s \right] [\beta \Delta f] = K_{pid} [\beta \Delta f] \quad (4)$$

Wind Turbine Model:

The wind farm model is modeled using the following transfer function.

$$\Delta P_W = \frac{1}{sT_{WT} + 1} \cdot (\Delta P_{Wind}) \quad (5)$$

PV Model:

The model of solar power is modeled using the following transfer function.

$$\Delta P_{PV} = \frac{1}{sT_{PV} + 1} \cdot (\Delta P_{solar}) \quad (6)$$

The SMES Model:

The SMES is simulated by the following transfer function based on a time constant (T_{SMES}) and SMES variable gain (K_{SMES}), obtained by the trial-and-error method.

$$\Delta P_{SMES} = \frac{K_{SMES}}{sT_{SMES} + 1} \cdot \left(\frac{d(\Delta f)}{dt} \right) \quad (7)$$

The overall dynamic equation of generator-demand between the total power and the frequency deviation considering the effect of both RES and SMES can be obtained as:

$$\Delta f = \frac{1}{2Hs + D} (\Delta P_m + \Delta P_W + \Delta P_{PV} \pm \Delta P_{SMES} - \Delta P_L) \quad (8)$$

The MG state space model is shown in Eq. (9) and Eq. (10).

$$X = Ax + B_1 w + B_2 u \quad (9)$$

$$y = Cx \quad (10)$$

where,

$$x^T = [\Delta f \cdot \Delta P_m \cdot \Delta P_g \cdot \Delta P_{ACE} \cdot \Delta P_W \cdot \Delta P_{PV} \cdot \Delta P_{SMES}] \quad (11)$$

$$w^T = \Delta P_{Wind} \cdot \Delta P_{solar} \cdot \Delta P_L \quad (12)$$

$$y = \Delta f \quad (13)$$

The complete state-space model of the studied MG regarding the impacts of RES and SMES is reported in [34] using the previous state variables from Eq. (1) to Eq. (10).

Complete SMES Model

Fig. 3 shows the schematic model of the SMES unit, which has a DC superconducting coil (SC), which is considered the heart of the SMES. This SC is connected to the AC grid through a power conversion system (PCS), which includes an inverter and a DC-DC chopper for inversion and rectification purposes. The SMES control operation during standby, charging, and discharging modes are achieved by applying zero, positive, and negative voltage, respectively to SC. This

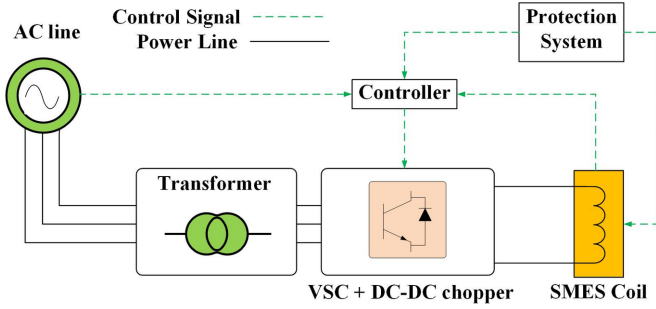


Figure 3: Detailed configuration of SMES in the power system

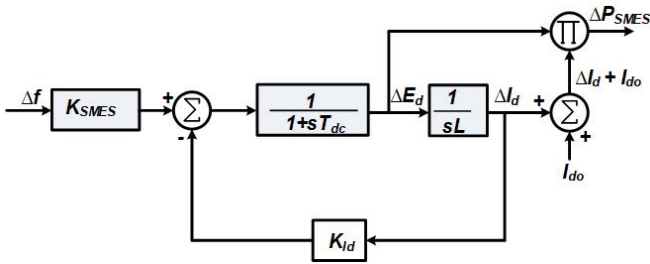


Figure 4: SMES control model as a frequency stabilizer [35]

occurs through the firing angle control of the converter circuit. The modeling of the SMES transfer function is illustrated in Fig. 4, where the area control error (ACE) is given to the gain (K_{SMES}) to derive the change in converter voltage (ΔE_d) as shown in Eq. (14). The incremental change in SC current (ΔI_d) is used as a negative feedback signal in the control loop of SMES to achieve rapid restoration of the SC current after any load disturbance [35].

$$\Delta E_d = \frac{K_{SMES}}{sT_{dc} + 1} \cdot \Delta f \quad (14)$$

where, ΔE_d is the incremental change in converter voltage, T_{dc} the converter time delay in a second; K_{SMES} is the gain of the SMES control loop. The SC inductor current deviation (ΔI_d) can be calculated by Eq. (15).

$$\Delta I_d = \frac{\Delta E_d}{sL} \quad (15)$$

The overall power change of SMES ΔP_{SMES} due to system frequency deviation (Δf) is determined by Eq. (16):

$$\Delta P_{SMES} = \Delta E_d \cdot I_d \quad (16)$$

$$I_d = I_{do} + \Delta I_d \quad (17)$$

where I_d is net SC inductor current.

Operation Strategy

This section discusses the operation strategy of SMES for the studied MG, with consideration given to RES and load variations. The operation flowchart is shown in Fig. 5. MG

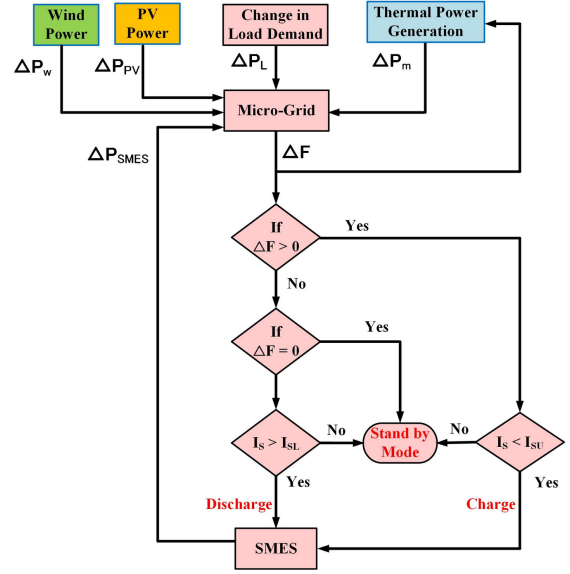


Figure 5: Flowchart of the SMES operation strategy

frequency changes whenever load disturbance occurs. However, system frequency must be maintained within allowable limits for stable MG operation. In order to stabilize the frequency fluctuations, generation must be controlled based on demand load changes. Therefore, frequency over or under 50 Hz must be detected. If the frequency is under 50 Hz and SC current I_d greater than the lower limit I_{dL} , SMES discharges power otherwise it endures in standby mode. If the frequency is over 50 Hz and I_d lower than its upper limit I_{dU} , SMES starts to charge power from the grid; otherwise, it remains in standby mode.

Proposed Coordination Strategy

SMES Based Optimal PID

The main target of this part is to design a robust SMES-based optimal PID controller to emulate the virtual inertia of the tested MG. This will support MG frequency and save it from collapse during large disturbances. Moreover, a recent swarm intelligence method called moth swarm algorithm (MSA) is applied to reduce the MG frequency deviations and produce the optimal PID parameter under different operating situations of the MG.

Control Problem Formulation

In this research, the proposed coordinated control strategy of SMES and LFC is based on the PID controller. The tuning of the PID controller depends on three parameters: proportional gain k_p , integral gain k_i and derivative gain k_d . These parameters are calculated through the moth swarm algorithm optimization technique. The actuating signal of the PID controller is the summation of three parameters of the error signal, as follows:

$$G_c(s) = K_p + \frac{K_i}{s} + K_d s \quad (18)$$

In order to achieve optimum system response, MSA tries to find the optimal PID controller by reducing the integral time squared-error (ISE), which is the objective function of the optimization technique and can be formulated as shown below:

$$ISE = \int_0^{t_s} (\Delta f)^2 dt \quad (19)$$

Table 2: PID controller parameters for MG

Parameter	Kp	Ki	Kd
Value	3.76	22.14	0.85

where Δf is the system frequency deviation and t_s is the simulation time. The proposed MSA is applied to minimize the objective function of the ISE subjected to the constraints of the PID controller parameters limits as in Eq. (20). Table 2 includes the optimal values of the PID gains.

$$\left\{ \begin{array}{l} K_{P \min} \leq K_P \leq K_{P \max} \\ K_{i \min} \leq K_i \leq K_{i \max} \\ K_{d \min} \leq K_d \leq K_{d \max} \end{array} \right\} \rightarrow (0 \sim 100) \quad (20)$$

Overview of MSA

In this paper, the MSA was adapted to find the optimum parameters of the PID controller by minimizing the objective function as given in Eq. (19). MSA is a new optimization algorithm, proposed by the authors Emad et al. in [36]. The MSA was established based on moth swarms flying by moonlight. A swarm of moths utilizes celestial navigation in order to be on a straight-line direction at night, for example when the flight path lies at a constant point to parallel lights of rays like a remote light source. In MSA, the near light source from moths acts as obstructions for them. The optimal solution of any problem is determined based on the relative position of the moth swarm to the moon, while the luminous intensity measured the solution quality. Each swarm consists of three groups [36], which are: (i) pathfinders that have the ability to discover new areas in the search space. They distinguish the best position of light sources to guide the swarm of the main groups; (ii) prospectors that fly into a spiral path close to the light sources, which have been marked by the pathfinders; and (iii) onlookers that fly directly towards the moonlight, which is the best global solution, as represented by the prospectors. The MSA is handled in four main phases as follows:

Phase of initialization: The initial positions of moths are randomly generated as follows:

$$\left\{ \begin{array}{l} x_{ij} = rand[0, 1] \cdot (x_j^{\max} - x_j^{\min}) + x_j^{\min} \\ i = \{1, 2, \dots, n\} \\ j = \{1, 2, \dots, d\} \end{array} \right. \quad (21)$$

where x_j^{\min} and x_j^{\max} represent the upper and lower limits, d is the dimension of the problem and n is the population number. After the initial process, the moths are divided into

different types based on the calculated fitness. The best type of moth are the pathfinders, the second are the prospectors and the worst are the onlookers.

Phase of reconnaissance: To improve the diversity index of the optimal solution, the crossover points are depicted based on a new strategy. At iteration t , the normalized dispersal degree is calculated as follows:

$$\sigma_j^t = \frac{\sqrt{\frac{1}{n_p} \sum_{i=1}^{n_p} (x_{ij}^t - \bar{x}_j^t)^2}}{\bar{x}_j^t} \quad (22)$$

where the pathfinder moths number is n_p , $\bar{x}_j^t = \frac{1}{n_p} \sum_{i=1}^{n_p} x_{ij}^t$, and the variation coefficient is $\mu^t = \frac{1}{d} \sum_{j=1}^d \sigma_j^t$.

Spiral movement of prospectors: The prospectors are the next best luminescence intensity group of moth swarms. The number of prospectors n_f that reduce during the iteration process can be mathematically calculated as follows:

$$n_f = round\left((n - n_p) \times \left(1 - \frac{t}{T}\right)\right) \quad (23)$$

The new position of the prospector moth (x_i) is updated by using Eq. (24) according to the spiral flight path for the next iteration.

$$\left\{ \begin{array}{l} x_i^{t+1} = |x_i^t - x_p^t| \cdot e^{\theta} \cdot \cos 2\pi\theta + x_p^t \\ \forall p \in \{1, 2, \dots, n_p\} \\ i \in \{n_p + 1, n_p + 2, \dots, n_f\} \end{array} \right. \quad (24)$$

where θ is a random number in $[r, 1]$ and equal to $(-1 - \frac{t}{T})$. Due to consistently changing the group of each moth, if there is more luminescence than the existing light sources, then they try to become a pathfinder moth.

Movement of onlookers: During the process in MSA method, the number of prospectors reduces and the number of onlookers increases in the search space. This may result in accelerating the convergence rate of the MSA to achieve a global solution. The onlooker moths have the worst luminescent sources. Hence, the purpose of the moths in this group is to move towards the most shining solution. They are classified into two parts, which are Gaussian distribution of steps and associative learning mechanism (ALM) with instant memory. The updating equation for the onlooker moth is created according to Gaussian walks and is defined as follows:

$$\left\{ \begin{array}{l} x_i^{t+1} = x_i^t + \varepsilon_1 + [\varepsilon_2 \times best_g^t - \varepsilon_3 \times x_i^t] \\ \forall i \in \{1, 2, \dots, n_G\} \end{array} \right. \quad (25)$$

$$\varepsilon_1 \sim random(size(d)) N\left(best_g^t, \frac{\log t}{t} \times (x_i^t - best_g^t)\right) \quad (26)$$

where ε_1 is a random sample drawn from Gaussian (Normal) distribution as a random sample and is the global best solution, ε_2 and ε_3 are uniformly distributed random numbers

within the range [0,1]. The updating equation for the new on-looker moth for the next generation is written on the basis of ALM with immediate rate term as follows:

$$x_i^{t+1} = x_i^t + 0.001 \cdot G \left[x_i^t - x_i^{min}, x_i^{max} - x_i^t \right] (1 - g/G) \cdot r_1 \cdot (best_p^t - x_i^t) + 2g/G \cdot r_2 (best_g^t - x_i^t) \quad (27)$$

Modeling of the DFR Scheme

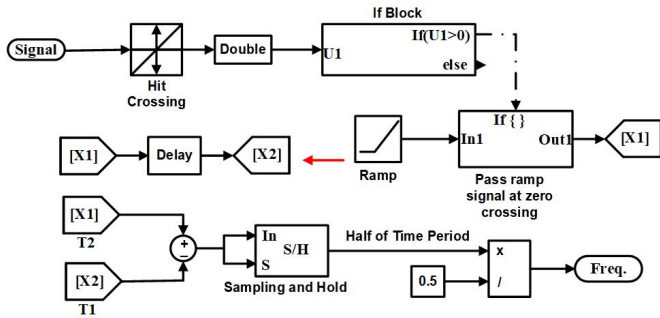


Figure 6: Frequency Measurement Unit (FMU)

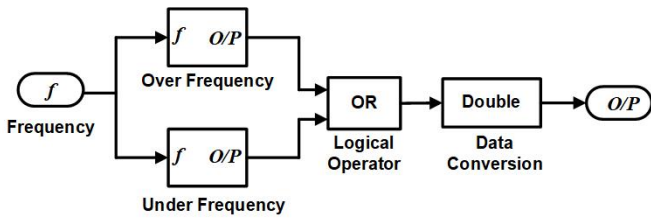


Figure 7: Frequency Detection Element (FDE)

Modelling of DFR: The detailed modeling of the DFR was presented by the authors in [37]. DFR is divided into two main components, the first portion is the Frequency Measuring Unit (FMU), which is used to measure the digital value of the system frequency using some logical operations as shown in the Matlab Simulink model of Fig. 6. Then the frequency detection element (FDE) receives the measured frequency signal to take action based on the DFR limit for necessary tripping. The output from frequency is logically OR. The output of FDE under the normal case is 1, otherwise 0 (for tripping) as shown in Fig. 7. According to the modeling for the DFR, it can be implemented by an intelligent electronic device (IED) using microprocessor-based technology. The design block offers flexibility in terms of further research and improvement.

Table 3: PID controller parameters for MG

System frequency	DFR	Limit range	Integrator value
50 Hz	Over	fmax = 51 Hz	K = 5 sec
	Under	fmin = 49 Hz	

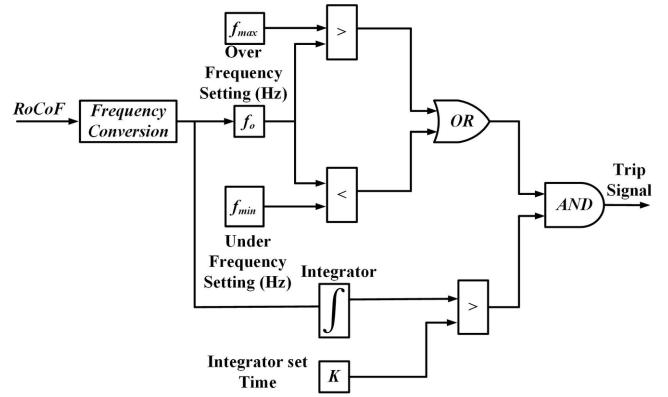


Figure 8: DFR model

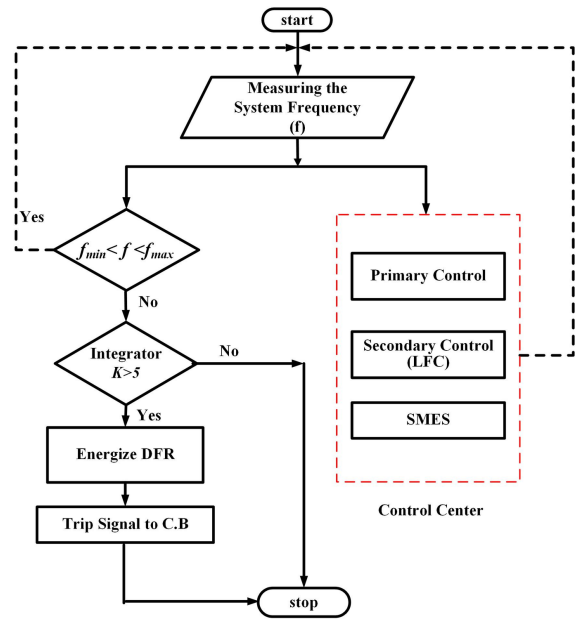


Figure 9: Flowchart of the overall operation

DFR Operation: The designed DFR in this work is shown in Fig. 8. The operation of the DFR depends on measuring the system frequency and comparing it with the frequency limits of the DFR ($f_{max} < f < f_{min}$). To energize the relay and then send a protection signal to the responsible circuit breaker, two conditions must be met together: (i) the system frequency exceeds the permissible limits of the over and under frequency setting, and (ii) the integrator output magnitude is larger than the threshold value ($K=5$ sec). On the other hand, the role of the LFC and SMES emerges when the measured frequency leaves the permissible limits and the integrator output magnitude does not exceed the integrator set time (K). As per the international grid code for the islanded-MG mode in Europe [37], the setting of the proposed DFR is indicated in Table 3. The operation of the digital DFR coordinated with LFC and SMES is represented in the flowchart of Fig. 9.

Results and Analysis

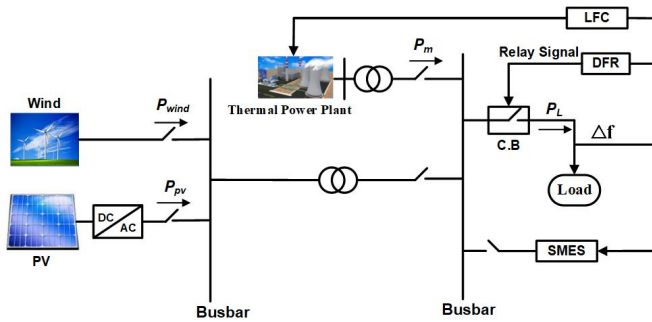


Figure 10: MG Single-line diagram

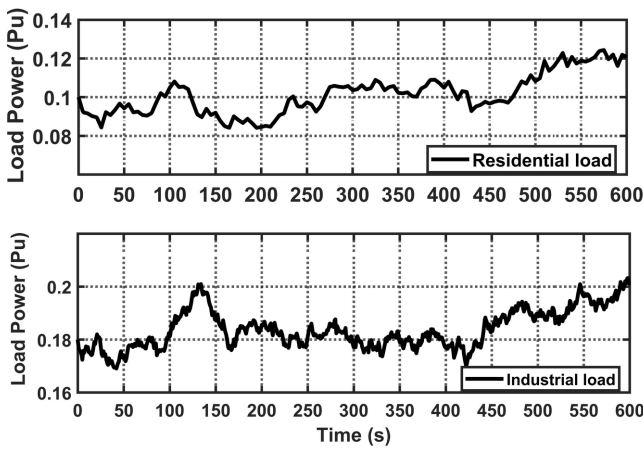


Figure 11: Power fluctuation of wind/solar generation units

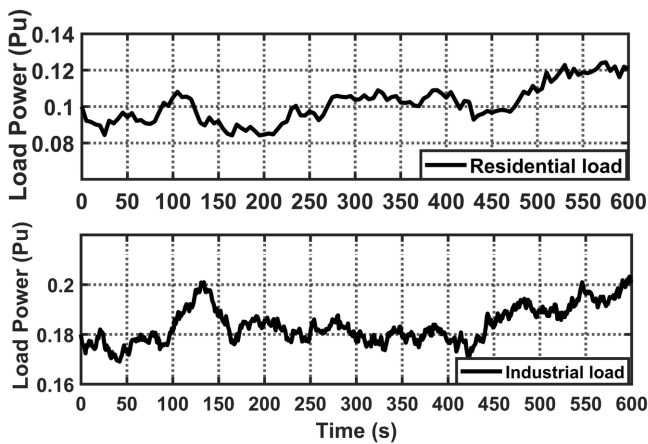


Figure 12: Random Load deviation

The proposed method of coordination between secondary control, SMES, and DRF for the MG is verified on the MG single-line diagram as shown in Fig. 10 during the intermittent/variable sources, radical load change (i.e. disturbances) and low inertia effect (i.e., system uncertainties). All simulation cases and analysis of the studied MG are executed

using MATLAB/Simulink in the presence of highly fluctuating wind power and solar power shown on Fig. 11, in addition to load variations as shown on Fig. 12 for simulation time of 10 minutes. Three scenarios are carried out to examine the dynamic security of the MG utilizing the proposed control/protection method of LFC and DFR as follows:

MG Performance Without RESs

Table 4: Multiple operating conditions of MG, Case 1

Source	Starting	Stopping	Size (pu)
Industrial load	150 sec	-	0.22
Residential load	initial	400 sec	0.12

The main objective of this section is to investigate MG performance with the proposed coordinated strategy of LFC, SMES, and DFR by implementing highly fluctuating residential and industrial loads with three different levels of system inertia. Table 4 summarizes the different disturbance conditions during this simulation.

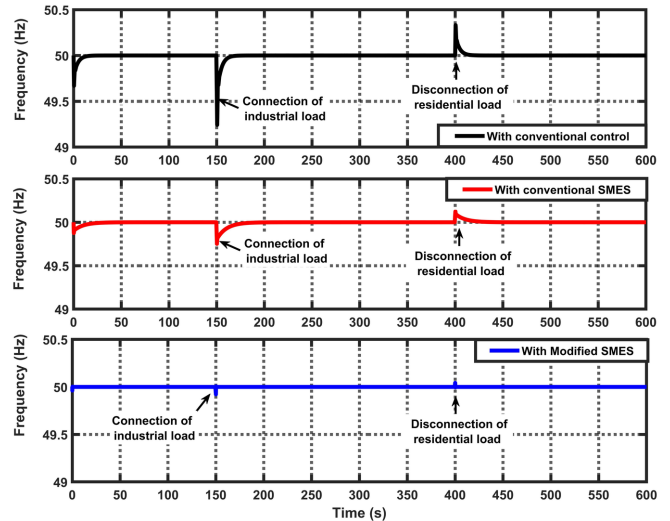


Figure 13: MG frequency response for Case 1A (100% of default system inertia)

Case 1A: In this case, the studied MG is examined under 100% of the default system inertia considering the random load variations of Table 4. Fig. 13 shows the MG frequency response in that case, where the frequency control loops succeeded to return the MG frequency with the three scenarios without any need from the protection scheme. Without SMES, the frequency change is about ± 0.74 Hz, while the conventional SMES damped the frequency variation to ± 0.25 Hz. The SMES based-optimal PID signal gave a very smooth frequency response to only ± 0.08 Hz when the high fluctuated industrial load is connected at 150 sec. This result is the best value compared to other methods in terms of overshoots/undershoots and settling time.

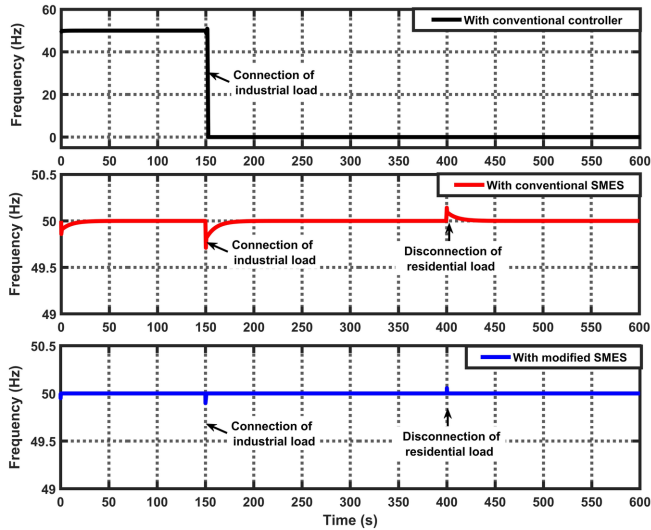


Figure 14: MG frequency for **Case 1B** (55% of default system inertia)

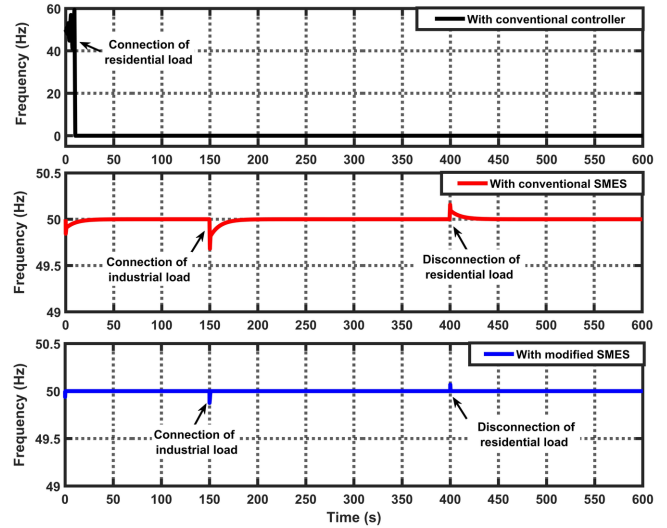


Figure 15: MG frequency response for **Case 1C** (35% of default system inertia)

Case 1B: In this case, the MG is subjected to the same operating conditions of Table 4, in addition to reducing system inertia to 55% of the default system inertia level. Fig. 14 shows the MG frequency response. It can be seen that the conventional controller cannot restore the MG frequency if the frequency deviation exceeded the allowable limits. Hence, the DFR energizes and sends a signal to the responsible circuit breaker to trip, because the integrator value (K) exceeds its threshold value at 150 sec when the industrial load is connected. While the conventional SMES damped the frequency variation to only ± 0.3 Hz at 150 sec and the DFR does not energize as the integrator threshold output magnitude does not override the specified value. On the other hand, the SMES based-optimal PID controller can maintain system frequency within ± 0.1 Hz during the connection of heavy industrial load at 150 sec under the critical low inertia case.

Case 1C: In this case, the MG is examined during an extreme scenario of very low inertia (35% of the default MG inertia) in addition to the previous load variation conditions of Table 4. The conventional controller cannot withstand the extreme low inertia case at the first disturbance step at initial operation and the DRF emerges sending a signal to the circuit breaker for tripping to protect the MG system from failure as depicted in Fig. 15. The MG response with the conventional SMES fluctuates beyond the allowable limits and maintains the frequency change around ± 0.32 Hz without the need of protective action. The modified SMES gave the best control performance in this extreme inertia scenario by immediately dumping the frequency fluctuation to ± 0.11 Hz. Therefore, the superiority of the proposed technique of modified SMES was approved to preserve the dynamic security in a low-inertia MG.

MG Performance with RESs

The main objective of this section is to investigate MG performance with the proposed coordinated strategy of LFC,

Table 5: Multiple operating conditions of the MG of Case 2

Source	Starting	Stopping	Size (pu)
Industrial load	150 sec	-	0.22
Residential load	initial	400 sec	0.12
Wind power	300 sec	-	0.23
PV	initial	-	0.15

SMES, and DFR by implementing high-fluctuated wind and PV variation, in addition to high-fluctuated residential and industrial load variations during three different levels of system inertia. Table 5 summarizes the different disturbance condition during this simulation.

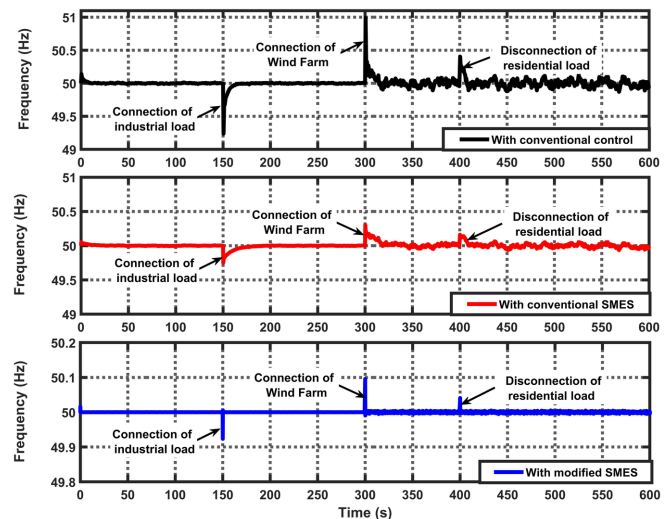


Figure 16: MG frequency for **Case 2A** (100% of default system inertia)

Case 2A: Fig. 16 shows the frequency response of the MG in the sequence of operating conditions as shown in Table 5 with inertia level (100% of default system inertia). In this

case, the conventional controller restored system frequency to 50 Hz, but with the high-frequency variation of ± 0.98 Hz, which is very near the maximum allowable limits and with long settling time during wind farm connection at 300 sec. The conventional SMES successfully maintained frequency fluctuation at around ± 0.31 Hz. However, it takes a long time to stabilize at 50 Hz. On the other hand, the proposed modified SMES based on the optimal PID controller damped the frequency oscillations to only ± 0.09 Hz with fast time compared to other methods. This case proved the effectiveness of the coordination strategy of LFC and SMES without any action from the DFR protection system.

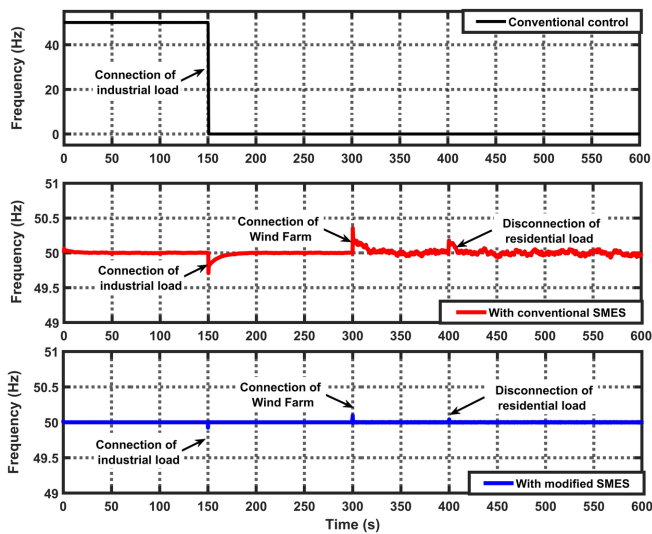


Figure 17: MG frequency for Case 2B (55% of default system inertia)

Case 2B: the MG system, in this case, is exposed to the same operating conditions of Table 5, in addition to reducing system inertia to 55% of the default system inertia level. Fig. 17 shows the MG frequency response in that case, where the conventional control failed to iterate the system frequency to its set value during connection of industrial load at 150 sec and at a low inertia value. Hence, the DRF emerged in this situation to protect the MG components from damage by sending a trip signal for protective action. The conventional SMES gave a frequency change of ± 0.36 Hz when the wind farm is connected at 300 sec. However, it still needs a long time to settle down to 50 Hz. When using the modified SMES, the system frequency variation enhanced to about ± 0.1 Hz with smooth and quick frequency response. Hence, the proposed coordination still has the best effectiveness for maintaining MG dynamic security.

Case 2C: In this case, an extreme test scenario was performed by subjecting the MG to reduce the system inertia to 35% from its initial value, in addition to the same operating conditions in Table 5. Fig. 18 shows that the DFR protection system is energized and sends a trip signal to the circuit breaker to trip the generation units when using the conventional controller only. This happened due to the frequency variation exceeding the acceptable limits and the integrator value of DFR exceeding its threshold value at the first dis-

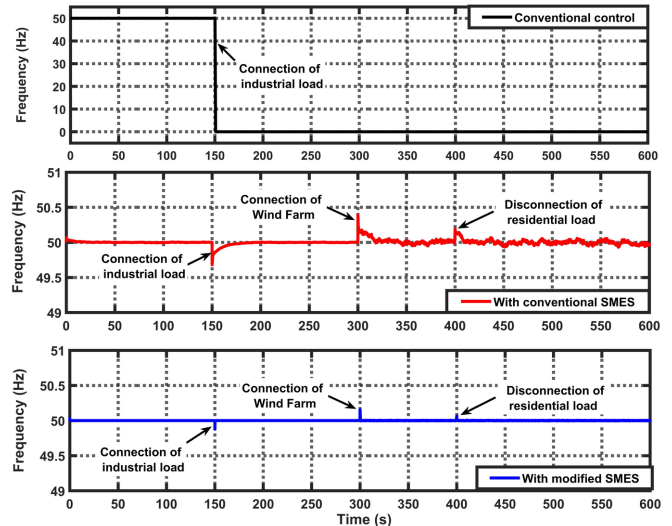


Figure 18: MG frequency for Case 2C (35% of default system inertia)

turbance operation at 150 sec. Hence, the DFR maintains system security in that case. While the conventional SMES damped the frequency oscillations to ± 0.39 Hz, the settling time was still somewhat long. On the other hand, the modified SMES-based optimal PID signal can reduce the frequency fluctuations rapidly to ± 0.15 Hz in that extreme inertia case, compared to the conventional controller and SMES as shown in Fig. 18.

Conclusion and Discussions

This paper proposed a coordination strategy of secondary control, SMES, and digital Frequency Relay (DFR) for enhancing the stability and protection of the low-inertia microgrid (MG), considering high levels of Renewable Energy Sources (RESs) penetration. The proposed SMES-based optimal PID controller, designed using new swarm intelligence of MSA, was applied to emulate inertia characteristics.

The simulation results proved that the proposed SMES-based optimal PID controller achieved robust frequency stability in the presence of high wind/PV power penetration. Different load power fluctuations and different levels of system inertia against all cases of studied scenarios in terms of peaks overshoot, peaks undershoot and settling time are considered in this work. These results have been compared with and without the conventional SMES, which needs a little longer time to suppress the frequency deviations compared with the proposed coordination. Furthermore, conventional and modified SMES have solved the interference problem between the frequency control and protection by damping the frequency fluctuations quickly.

References

[1] Hassan Bevrani, Masayuki Watanabe, and Yasunori Mitani, editors. *Power System Monitoring and Control*. John Wiley & Sons Inc., may 2014.

- [2] Thomas Ackermann, editor. *Wind Power in Power Systems*. John Wiley & Sons Ltd, jan 2005.
- [3] Petros Aristedou, Gustavo Valverde, and Thierry Van Cutsem. Contribution of Distribution Network Control to Voltage Stability: A Case Study. *IEEE Transactions on Smart Grid*, 8(1):106–116, jan 2017.
- [4] Jingjing Zhao, Xue Lyu, Yang Fu, Xiaoguang Hu, and Fangxing Li. Coordinated Microgrid Frequency Regulation Based on DFIG Variable Coefficient Using Virtual Inertia and Primary Frequency Control. *IEEE Transactions on Energy Conversion*, 31(3):833–845, sep 2016.
- [5] Salvatore D’Arco, Jon Are Suul, and Olav B. Fosso. Small-signal modeling and parametric sensitivity of a virtual synchronous machine in islanded operation. *International Journal of Electrical Power & Energy Systems*, 72:3–15, nov 2015.
- [6] Ujjwol Tamrakar, Dipesh Shrestha, Manisha Maharjan, Bishnu Bhattarai, Timothy Hansen, and Reinaldo Tonkoski. Virtual Inertia: Current Trends and Future Directions. *Applied Sciences*, 7(7):654, jun 2017.
- [7] Jia Liu, Yushi Miura, and Toshifumi Ise. Comparison of Dynamic Characteristics Between Virtual Synchronous Generator and Droop Control in Inverter-Based Distributed Generators. *IEEE Transactions on Power Electronics*, 31(5):3600–3611, may 2016.
- [8] Thongchart Kerdphol, Fathin Rahman, Yasunori Mitani, Komsan Hongesombut, and Sinan Küfeoğlu. Virtual Inertia Control-Based Model Predictive Control for Microgrid Frequency Stabilization Considering High Renewable Energy Integration. *Sustainability*, 9(5):773, may 2017.
- [9] Ruifeng Yan and Tapan Kumar Saha. Frequency response estimation method for high wind penetration considering wind turbine frequency support functions. *IET Renewable Power Generation*, 9(7):775–782, sep 2015.
- [10] Konstantina Mentessidi, Raquel Garde, Monica Aguado, and Evangelos Rikos. Implementation of a fuzzy logic controller for virtual inertia emulation. In *2015 International Symposium on Smart Electric Distribution Systems and Technologies (EDST)*. IEEE, sep 2015.
- [11] Yalong Hu, Wei Wei, Yonggang Peng, and Jinyong Lei. Fuzzy virtual inertia control for virtual synchronous generator. In *2016 35th Chinese Control Conference (CCC)*. IEEE, jul 2016.
- [12] Miguel A. Torres L., Luiz A. C. Lopes, Luis A. Moran T., and Jose R. Espinoza C. Self-Tuning Virtual Synchronous Machine: A Control Strategy for Energy Storage Systems to Support Dynamic Frequency Control. *IEEE Transactions on Energy Conversion*, 29(4):833–840, dec 2014.
- [13] Anamika Yadav Bokka Krishna Chaitanya, Atul Kumar Soni. Communication Assisted Fuzzy based Adaptive Protective Relaying Scheme for Microgrid. *Journal of Power Technologies*, 98, 2018.
- [14] Hassan Bevrani. Robust PI-Based Frequency Control. In *Robust Power System Frequency Control*, pages 71–104. Springer International Publishing, 2014.
- [15] Sergio Vazquez, Srdjan M. Lukic, Eduardo Galvan, Leopoldo G. Franquelo, and Juan M. Carrasco. Energy Storage Systems for Transport and Grid Applications. *IEEE Transactions on Industrial Electronics*, 57(12):3881–3895, dec 2010.
- [16] Andreas Poullikkas Pavlos Nikolaidis. A comparative review of electrical energy storage systems for better sustainability. *Journal of Power Technologies*, 97 No 3, 2017.
- [17] Wei Li and Geza Joos. Comparison of Energy Storage System Technologies and Configurations in a Wind Farm. In *2007 IEEE Power Electronics Specialists Conference*. IEEE, 2007.
- [18] Abraham Ellis, David Schoenwald, Jon Hawkins, Steve Willard, and Brian Arellano. PV output smoothing with energy storage. In *2012 38th IEEE Photovoltaic Specialists Conference*. IEEE, jun 2012.
- [19] Ujjwol Tamrakar, David Galipeau, Reinaldo Tonkoski, and Indraman Tamrakar. Improving transient stability of photovoltaic-hydro microgrids using virtual synchronous machines. In *2015 IEEE Eindhoven PowerTech*. IEEE, jun 2015.
- [20] Ming Ding and Jie Wu. A Novel Control Strategy of Hybrid Energy Storage System for Wind Power Smoothing. *Electric Power Components and Systems*, 45(12):1265–1274, jul 2017.
- [21] Jie Dang, John Seuss, Luv Suneja, and Ronald G. Harley. SoC Feedback Control for Wind and ESS Hybrid Power System Frequency Regulation. *IEEE Journal of Emerging and Selected Topics in Power Electronics*, 2(1):79–86, mar 2014.
- [22] Jun Yeong Yun, Garam Yu, Kyung Soo Kook, Do Hwan Rho, and Byung Hoon Chang. SOC-based Control Strategy of Battery Energy Storage System for Power System Frequency Regulation. *The Transactions of the Korean Institute of Electrical Engineers*, 63 No 5, 2014. Accessed on Mon, September 23, 2019.
- [23] Marcelo G. Molina, Pedro E. Mercado, and Edson H. Watanabe. Static synchronous compensator with superconducting magnetic energy storage for high power utility applications. *Energy Conversion and Management*, 48(8):2316–2331, aug 2007.
- [24] T. Kinjo, T. Senjyu, N. Urasaki, and H. Fujita. Terminal-voltage and output-power regulation of wind-turbine generator by series and parallel compensation using SMES. *IEE Proceedings - Generation Transmission and Distribution*, 153(3):276, 2006.
- [25] Praghnes Bhatt, S.P. Ghoshal, and Ranjit Roy. Coordinated control of TCPS and SMES for frequency regulation of interconnected restructured power systems with dynamic participation from DFIG based wind farm. *Renewable Energy*, 40(1):40–50, apr 2012.
- [26] M. Abdel-Akher Sayed M. Said, Mohamed M. Aly. Application of Superconducting Magnetic Energy Storage (SMES) to Improve Transient Stability of Multi-Machine System with Wind Power Penetration. In *16th International Middle East Power Systems Conference (MEP-CON), Cairo, Egypt, 2014*, pp. 1-6., 2014.
- [27] Mohamed M. Aly, Mamdouh Abdel-Akher, Sayed M. Said, and Tomonobu Senjyu. A developed control strategy for mitigating wind power generation transients using superconducting magnetic energy storage with reactive power support. *International Journal of Electrical Power & Energy Systems*, 83:485–494, dec 2016.
- [28] Emad A. Mohamed, E. Gouda, and Yasunori Mitani. Impact of SMES integration on the digital frequency relay operation considering High PV/Wind penetration in micro-grid. *Energy Procedia*, 157:1292–1304, jan 2019.
- [29] J.A. Laghari, H. Mokhlis, A.H.A. Bakar, and Hasmaini Mohamad. Application of computational intelligence techniques for load shedding in power systems: A review. *Energy Conversion and Management*, 75:130–140, nov 2013.
- [30] Hamdy Ahmed Ashour Ayatte Ibrahim Atteya, Amani Mohamed El Zonkoly. Adaptive protection scheme for optimally coordinated relay setting using modified PSO algorithm. *Journal of Power Technologies*, 97 No 5, pp. 463–469., 2017.
- [31] Naowarat Tephiruk, Komsan Hongesombut, Yuthasak Urathamakul, Sirivat Poonvasin, and Sane Tangsatit. Modeling of rate of change of under frequency relay for microgrid protection. In *2017 International Electrical Engineering Congress (IEECON)*. IEEE, mar 2017.
- [32] W. Freitas, W. Xu, C.M. Afonso, and Z. Huang. Comparative Analysis Between ROCOF and Vector Surge Relays for Distributed Generation Applications. *IEEE Transactions on Power Delivery*, 20(2):1315–1324, apr 2005.
- [33] J.C.M. Vieira, W. Freitas, W. Xu, and A. Morelato. Efficient Coordination of ROCOF and Frequency Relays for Distributed Generation Protection by Using the Application Region. *IEEE Transactions on Power Delivery*, 21(4):1878–1884, oct 2006.
- [34] Gaber Magdy, Emad A. Mohamed, G. Shabib, Adel A. Elbaset, and Yasunori Mitani. SMES based a new PID controller for frequency stability of a real hybrid power system considering high wind power penetration. *IET Renewable Power Generation*, 12(11):1304–1313, aug 2018.
- [35] Shailendra Singh, Rohit Kumar Verma, Ashish Kumar Shakya, and Satyendra Pratap Singh. Frequency Regulation of Micro-grid Connected Hybrid Power System with SMES. *Technology and Economics of Smart Grids and Sustainable Energy*, 2(1), jul 2017.
- [36] Emad Mohamed Younis, Mohamed Al-Attar, Thongchart Kerdphol, and Yasunori Mitani. Optimization of Reactive Compensation in Distribution Networks Based on Moth Swarm Intelligence for Multi-Load Levels. *International Review of Electrical Engineering (IREE)*, 12(4):342, aug 2017.
- [37] Emad A. Mohamed, Gaber Magdy, Gaber Shabib, Adel A. Elbaset, and Yasunori Mitani. Digital coordination strategy of protection and frequency stability for an islanded microgrid. *IET Generation Transmission & Distribution*, 12(15):3637–3646, aug 2018.